Second Harmonic Generation in Optical Waveguides

Keywords: Nonlinear Optics, Second Harmonic Generation, MoS_2

Authors:
Otávio Rodrigues de Oliveira, IFGW - Unicamp
Prof. Dr. Gustavo S. Wiederhecker (advisor), IFGW - Unicamp

Introduction

Nonlinear optical interactions in monolayer transition-metal dichalcogenides (TMDCs), such as MoS_2, have drawn considerable interest in the past decade [1, 2, 3]. These 2D materials are particularly important for second-harmonic generation (SHG), as they are noncentrosymmetric.

However, in the majority of the experiments performed to date, the TMDCs are pumped with a high intensity pulsed laser at normal incidence, which limits the nonlinear interaction to the laser spot size. Aiming at enhancing the conversion efficiency of SHG in MoS_2 with the pump at 1550 nm, we propose a design where the MoS_2 monolayer is transferred onto a waveguide integrated on a chip. With this design, we can significantly increase the interaction length of light with the 2D material.

The initial goal of this scientific initiation project was to address phase-matching constraints through the concept of quasi-phase-matching strategy, which is achieved by setting up an array of evenly spaced MoS_2 microribbons over the waveguide, as shown in Fig. 1(a). In collaboration with a post-doctoral researcher and researchers at MackGraphe (Mackenzie University), we aim to develop theoretical and experimental progress towards efficient SHG in MoS_2. This patterning layout will be accomplished with lithographic and etching processes [4]. The on-chip integrated waveguides used in this analysis were already fabricated using commercially lithographic process offered by Ligentec SA. Their key features are displayed in fig. 1(a). At the end of research period, only theoretical progress towards the modeling of second harmonic phenomena on MoS_2 was obtained, with experimental procedure still to be implemented.

Methods

Theoretical modeling

To determine the micro-ribbon size and orientation of the MoS_2 monolayer for a given pair of waveguide modes, we've modeled the SHG process with nonlinear coupled equations in the slowly varying amplitude approximation (SVEA) [5]. In this treatment, the electric field in the waveguide is described as:

$$\vec{E} = \sum_j a_j(z)\, \vec{e}_j(x,y)\, \exp\left(i\beta_j z\right), \tag{1}$$

where $a_j(z)$, $\vec{e}_j(x,y)$ and β_j are, respectively, the slowly varying envelope, the field profile and the propagation constant of the j-th mode. Using the mode expansion strategy, the equation describing the evolution of the second harmonic field can be derived following a perturbation theory approach to Maxwell's wave equations in matter. It can be written as:

$$\frac{\partial a_{SH}}{\partial z} = i\frac{\omega_{SH}}{4\mathcal{N}_{SH}}\left[\int \vec{e}^{\,*}_{SH} \cdot \vec{P}_{SH}\, da\right] \exp\left(-i\,\beta_{SH} z\right), \tag{2}$$

with

$$\mathcal{N}_{SH} = \frac{1}{2}\int \vec{e}^{\,*}_{SH} \times \vec{h}_{SH} \cdot \hat{z}\, da \tag{3}$$

and

$$P_{SH}(2\omega) = \varepsilon_0 \sum_{j,k} \chi^{(2)}_{ijk}(2\omega;\omega,\omega) E_j(\omega) E_k(\omega) \tag{4}$$

where $\vec{h}_{SH}$, ω_{SH} and β_{SH} are, respectively, the magnetic field, angular frequency and propagation constant of the second-harmonic mode, z is the direction of propagation along the waveguide, the indices ijk refer to the Cartesian components of the fields, ε_0 denotes the vacuum permittivity and $\chi^{(2)}_{ijk}$ denotes the second-order susceptibility tensor. The field overlap integral of eq. (2) is performed over the domain of the nonlinear medium.

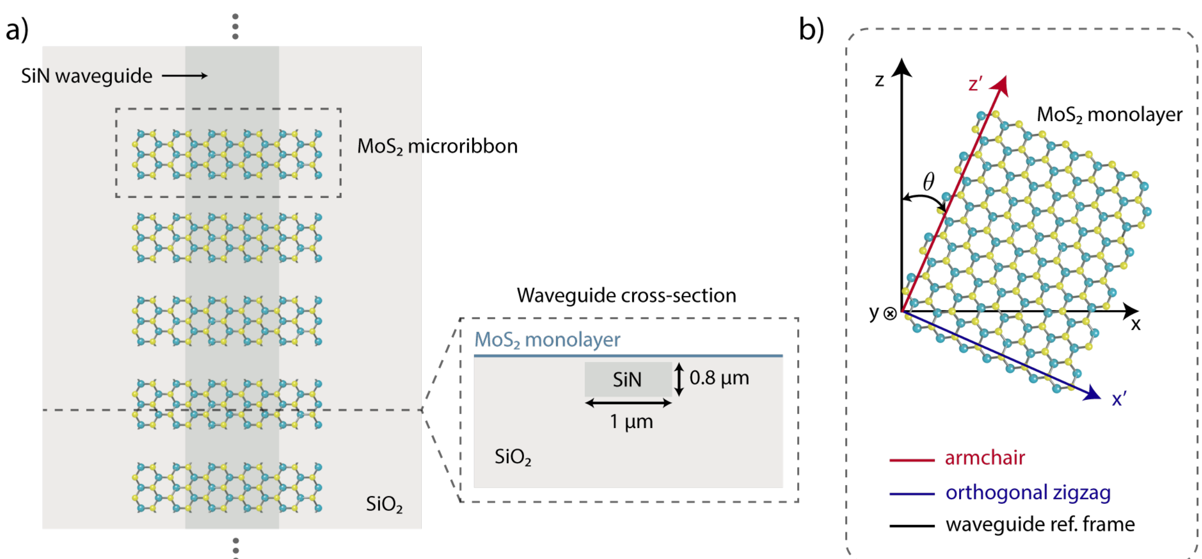

Figure 1: (a) Depicted view of a SiN waveguide integrated with an array of equally spaced MoS_2 microribbons used in the simulations. In this chip design, there is a 100 nm SiO_2 layer between the top surface of the waveguide and the MoS_2 microribbons. (b) Representation of the waveguide reference frame along with the MoS_2 crystal axes.

Given that the crystalline structure of MoS_2 belongs to the symmetry group $\mathcal{D}_{3h}$ and using Neumann's Principle, the transformation of the susceptibility tensor yielded only four non vanishing components [6, 7]:

$$\chi^{(2)} := \chi^{(2)}_{z'z'z'} = -\chi^{(2)}_{z'x'x'} = -\chi^{(2)}_{x'z'x'} = -\chi^{(2)}_{x'x'z'}, \tag{5}$$

where z' and x' are, respectively, the armchair and the orthogonal zigzag directions of the MoS_2 monolayer, as indicated in Fig. 1(b).

With the symmetry considerations of eq. (5), the integrand of eq. (2) written in the waveguide reference frame becomes:

$$\vec{e}^{\,*}_{SH} \cdot \vec{P}_{SH} = \varepsilon_0\, \chi^{(2)}\, a_F^2\, \exp{(i\, 2\beta_F\, z)}\, \Omega, \tag{6}$$

with:

$$\begin{aligned} \Omega = & [e^*_{SH,z}\; e^2_{F,z} - e^*_{SH,z}\; e^2_{F,x} - 2\, e^*_{SH,x}\; e_{F,z}\; e_{F,x}]\, cos(3\theta) + \\ & [e^*_{SH,x}\; e^2_{F,z} - e^*_{SH,x}\; e^2_{F,x} + 2\, e^*_{SH,z}\; e_{F,z}\; e_{F,x}]\, sin(3\theta), \end{aligned} \tag{7}$$

where $e_{SH,z}(e_{SH,x})$ is the second-harmonic field profile in the $z(x)$ direction, $e_{F,z}(e_{F,x})$ is the fundamental field profile in the $z(x)$ direction, and a_F and β_F are, respectively, the slowly varying envelope and propagation constant of the fundamental field.

To represent the array of evenly spaced MoS_2 microribbons, the second-order susceptibility can be described in terms of a Fourier series [5]. Taking only the first order contribution to the Fourier series and adding an offset to account for the empty spaces between the MoS_2 microribbons, we got:

$$\chi_{eff}(z) = \chi^{(2)}\, \frac{2}{\pi} \left[\frac{1 + \exp{(i \frac{2\pi}{\Lambda} z)}}{2} \right], \tag{8}$$

in which Λ is the optimum period for quasi-phase-matching:

$$\Lambda = \frac{2\pi}{\Delta\beta}. \tag{9}$$

with $\Delta\beta = |2\beta_F - \beta_{SH}|$ being the phase-mismatch factor between the fundamental and second-harmonic modes.

The conversion efficiency for SHG was obtained by solving eq. (1) in the undepleted pump regime, taking into account the symmetry considerations of eq. (5) and the effective second-order susceptibility introduced in eq. (8). It is given by:

$$\eta = \frac{P_{SH}}{{P_F}^2} = \frac{2\pi^2 c^2 \varepsilon_0^2\, {\chi^{(2)}}^2}{\lambda_F} \frac{\left| \int_{MoS_2} \Omega\, da \right|^2}{\left[\frac{1}{2} \int_S \vec{e}^{\,*}_{SH} \times \vec{h}_{SH} \cdot \hat{z}\, da \right] \left[\frac{1}{2} \int_S \vec{e}^{\,*}_{F} \times \vec{h}_{F} \cdot \hat{z}\, da \right]^2} \; |\gamma|^2, \tag{10}$$

with:

$$\gamma = \int_0^L \left[1 + \exp\left(i \frac{2\pi}{\Lambda} z \right) \right] \exp{(i \Delta\beta z)}\, dz, \tag{11}$$

in which, $Pot_{SH} = |a_{SH}|^2$, $Pot_F = |a_F|^2$, c is the speed of light in vacuum and λ_F is the fundamental field wavelength. In eq.(10), the integral in the numerator is performed only in the MoS_2 domain, whereas the integrals in the denominator are evaluated over the waveguide cross section (S).

The field overlap integrals of eq. (10) for a SiN waveguide buried in a SiO_2 substrate can be calculated using in Comsol Multiphysics. The field components of the fundamental and second-harmonic modes at 1550 and 775 nm, respectively, are calculated through a mode analysis study performed in a 2D component, where the waveguide cross-section is defined. The fundamental field was chosen to be the TE_{00}. Once the field solutions had been found, the fundamental and second-harmonic modes were projected onto another 2D geometry with the waveguide cross-section, so that their field overlap integrals could be performed. The mode projection is done with the aid of Comsol extrusion operators [8]. The propagation losses were neglected in the simulation, since they cut off only a very small fraction of the output power in millimetric-range interaction lengths ($\alpha = 0.2$ dB/cm as informed by Ligentec). A Mathematica script was implemented to calculate the conversion efficiency (eq. (10)), taking into account the field overlap factors obtained in Comsol and the phase-mismatch factor (γ). The second-order susceptibility considered in the calculations was 2.4×10^{-20} m^2/V [3].

Interaction	θ	**Conv. efficiency (W^{-1})**	$\Delta\beta$ **(rad/μm)**	**TE fraction**
$TE_{00} \rightarrow TM_{01}$	$0°$	4.51×10^{-13}	0.173	0.006
$TE_{00} \rightarrow TE_{01}$	$30°$	4.71×10^{-14}	0.394	0.956

Table 1: Main characteristics of the mode interactions that result in the highest conversion efficiencies for SHG in a SiN waveguide integrated with MoS_2. θ is the angle between MoS_2 armchair direction and the waveguide axis, $\Delta\beta$ is the phase-mismatch factor between the SH and fundamental field modes, and TE fraction is the fraction of the $\vec{e}_{SH}$-field in the x direction.

The SH modes that yield the highest overlap factors with the fundamental field mode in the MoS_2 domain, and therefore the highest conversion efficiency, were found to be the TM_{01} and TE_{01} modes. Their main characteristics are summarized in Table 1. The angle dependence of the conversion efficiency of the interactions $TE_{00} \rightarrow TM_{01}$ and $TE_{00} \rightarrow TE_{01}$, which is explicitly accounted for in eq (7). Note that the maximum conversion efficiency for the $TE_{00} \rightarrow TM_{01}$ interaction occurs for the MoS_2 armchair direction aligned along the waveguide, whereas for the $TE_{00} \rightarrow TE_{01}$ interaction it occurs when the airmchair direction forms a 30° angle with the waveguide axis. At first glance, it may seem odd that the highest conversion efficiency occurs for the $TE_{00} \rightarrow TM_{01}$ interaction, since the second-order susceptibility does not couple field components to the out-of-plane direction. Although the TM_{01} mode exhibits negligible field amplitude in the x-direction, its field component along the z-direction (waveguide axis) overlaps significantly with the TE_{00} mode in the MoS_2 domain. In this case, the high conversion efficiency is brought by the dominant $[e^*_{SH,z}\ e^2_{F,x}\ cos(3\theta)]$ term of eq. (7).

To ensure quasi-phase-matching to the $TE_{00} \rightarrow TM_{01}$ ($TE_{00} \rightarrow TE_{01}$) interaction, the width of the MoS_2 microribbons ($\Lambda/2$) should be 18 μm (8 μm). In the phase-mismatch condition, the MoS_2 layer is left unpatterned. After 1 mm of interaction length, the output SH-field power in the quasi-phase-matching regime is 60 nW, 3 orders of magnitude higher than the peak power achieved in the phase-mismatch regime. This SH-power level is also 3 orders of magnitude higher than that achieved by pumping the MoS_2 flake at normal incidence with a free-space laser [3].

Preliminary results of the MoS_2 transfer

Our collaborators in MackGraphe - SP have started the MoS_2 tranfer process to the waveguides fabricated by Ligentec. They have been able to transfer two uniform MoS_2 flakes onto different sections of the same SiN waveguide. Taking the two flakes into account, the total interaction length along the waveguide axis is around 100 μm, which we believe to be enough to evaluate the enhancement of the SH-power with the MoS_2 patterning.

By performing polarization-resolved SHG experiments [9], they have shown that the armchair direction of the transferred flakes form a 40° and a 35° angle with the waveguide axis, which makes them more suitable to SHG via the $TE_{00} \rightarrow TE_{01}$ interaction. Their small angle mismatch to the target 30° could lead to a decrease of at most 15% in the SH-output power, as evaluated by the angle-dependent power plots. The next steps would be to lithographically pattern the MoS_2 flakes to define the array of microribbons with 8 μm of width and perform the SHG measurements.

Final Considerations

Much on the experimental aspect has to be done to test the theoretical modeling of the problem. Still, with the preliminary results we've got a good insight on the main parameters and their impacts on the conversion efficiency of SHG process.

Further investigation on other possible geometry optimizations and interaction strength with waveguides geometric parameters are encouraged to deeper improvement and technical dominance of the effect studied. Other TMDC's monolayers, like WSe_2 and WS_2, may also be used to characterize the method and apparatus applicability on other contexts [10].

References

[1] Vincent Pelgrin et al. "Boosting the SiN nonlinear photonic platform with transition metal dichalcogenide monolayers". In: *Optics Letters* 47.4 (2022), pp. 734–737.

[2] Haitao Chen et al. "Enhanced second-harmonic generation from two-dimensional MoSe2 on a silicon waveguide". In: *Light: Science & Applications* 6.10 (2017), e17060–e17060.

[3] RI Woodward et al. "Characterization of the second-and third-order nonlinear optical susceptibilities of monolayer MoS2 using multiphoton microscopy". In: *2D Materials* 4.1 (2016), p. 011006.

[4] Daniel Rodrigo et al. "Mid-infrared plasmonic biosensing with graphene". In: *Science* 349.6244 (2015), pp. 165–168.

[5] Robert W Boyd. *Nonlinear optics*. Academic press, 2020.

[6] Martin Weismann and Nicolae C Panoiu. "Theoretical and computational analysis of second-and third-harmonic generation in periodically patterned graphene and transition-metal dichalcogenide monolayers". In: *Physical Review B* 94.3 (2016), p. 035435.

[7] R.C. Powell. *Symmetry, Group Theory, and the Physical Properties of Crystals*. Lecture Notes in Physics. Springer New York, 2010. ISBN: 9781441975980. URL: https://books.google.com.br/books?id=ojq5BQAAQBAJ.

[8] *Examples of the General Extrusion Operator*. https://www.comsol.com/support/learning-center/article/Examples-of-the-General-Extrusion-Operator-33651. Accessed: 2022-04-10.

[9] Pilar G Vianna et al. "Second-harmonic generation enhancement in monolayer transition-metal dichalcogenides by using an epsilon-near-zero substrate". In: *Nanoscale Advances* 3.1 (2021), pp. 272–278.

[10] Xinglin Wen, Zibo Gong, and Dehui Li. "Nonlinear optics of two-dimensional transition metal dichalcogenides". In: *InfoMat* 1.3 (2019), pp. 317–337. DOI: https://doi.org/10.1002/inf2.12024. eprint: https://onlinelibrary.wiley.com/doi/pdf/10.1002/inf2.12024. URL: https://onlinelibrary.wiley.com/doi/abs/10.1002/inf2.12024.